Acta Crystallographica Section A
Foundations of Crystallography
ISSN 0108-7673

Received 30 January 2003
Accepted 30 July 2003

Structure and bonding in α-copper phthalocyanine by electron diffraction

J. S. Wu* and J. C. H. Spence

Department of Physics and Astronomy, Arizona State University, Tempe, AZ 85287-1504, USA. Correspondence e-mail: jinsong.wu@asu.edu

Energy-filtered quantitative electron diffraction at liquid nitrogen temperature has been used to examine the atomic structure and bonding of metastable α-Cu phthalocyanine crystals. Three theoretical methods (kinematic, kinematic with excitation errors and Bloch wave) were employed for the intensity calculations. The Bloch-wave method was found to account for dynamical effects by greatly reducing the residual factor between experimental and simulated results. A new method for calculating electron scattering factors for partially charged ions is proposed and the sensitivity of electron diffraction to charge transfer is discussed. The atomic charge states were analyzed for α-Cu phthalocyanine using a charge cloud model in which the Gaussian bond charge is positioned along the bonds. Spot patterns were collected in the Kohler mode at two beam energies to reduce error. Using the best-fitting model, a deformation charge-density map is produced and compared to the neutral-atom model. From this, the main features of atomic charge transfer in the α-Cu phthalocyanine structure can be seen in the (010) plane.

1. Introduction

Depending on preparation conditions, copper phthalocyanine has many polymorphs among which α and β are two important structures. The structure of β-Cu phthalocyanine (a = 1.96, b = 0.479, c = 1.46 nm and β = 120.6°; space group $P2_1/a$) has been determined by X-ray diffraction (Brown, 1968*a*). The history of the α-Cu phthalocyanine (α-CuPc) structure is more complicated since it is metastable. The lattice parameters were first determined as tetragonal with a = 1.7367 and b = 1.279 nm (Robinson & Klein, 1952). Later, it was shown that a monoclinic cell with a = 2.592, b = 0.379, c = 2.392 nm and β = 90.4° (space group $C2/c$) was a better fit (Ashida *et al.*, 1966; Brown, 1968*b*). Although high-resolution electron-microscope imaging has been shown to be a powerful tool in studying the structure (Uyeda *et al.*, 1965; Murata *et al.*, 1976), radiation damage is known to have a more serious effect on imaging than diffraction (Clark *et al.*, 1979). Furthermore, direct methods can greatly enhance the applicability of electron diffraction. Dorset & Hauptman (1976) were the first to apply direct methods to electron diffraction data and the first test of direct methods to n-beam dynamical electron diffraction data was published by Dorset *et al.* (1979).

Electron microscopy has many advantages for the study of metastable nanostructures. Electron diffraction patterns, unaffected by lens aberrations, induce less radiation damage than electron-microscope images, and may be interpreted quantitatively for small thicknesses of organic films, especially if elastic energy filtering and well characterized area-detector systems are used (Zuo, 2000). We have therefore used a LEO 912 microscope with energy filter to collect diffraction patterns of thermally deposited CuPc crystals on a substrate of NaCl. The aim is to examine its structure, especially which modification was formed.

The sensitivity of transmission electron diffraction patterns to the details of the electrostatic potential (and hence the charge density) in crystals was pointed out many years ago (Cowley & Rees, 1947). Recently, electron diffraction has shown its ability to visualize the charge status of atoms in inorganic crystals (Zuo *et al.*, 1988; Spence & Zuo, 1992; Zuo *et al.*, 1999) and protein macromolecule crystals (Mitsuoka *et al.*, 1999; Zhong *et al.*, 2002). Hence a second aim of our work is to study the effect of charge redistribution in an α-CuPc crystal by electron diffraction. The scattering of an electron is determined by the total electrostatic potential in a crystal and the potential is sensitive to bonding effects. The redistribution of the negative charge affects the electron scattering factor, *i.e.* for ions of a light atom the scattering factor at zero angle (s = 0) deviates greatly from the usual estimate for a neutral atom, which depends on the atomic number (Vainshtein, 1964; O'Keeffe & Spence, 1994). The assumption of spherical, isolated and neutral atoms has been the basis for calculations of the electron structure factor and this is a good approximation for heavier atoms, for which the valence shell forms a minor part. However, for a light atom such as hydrogen which has no inner shells, the effect of bonding is very large. It is thus

known that the deviation of low-angle structure factors for organic crystals is much larger than that of inorganic crystals when bonding effects are taken into account.

It is well known that the parameterization of bond charge in crystals is not unique since it depends on the partitioning scheme used between atoms. The total ground-state charge density is formally independent of the basis functions used to expand the many-particle wavefunction. Yet many useful schemes have been devised, including the well established multipole expansion (Hansen & Coppens, 1978). We adopt in this work the non-atom-centered deformation model proposed by Brill (1960), Hellner (1977) and coworkers (Dietrich & Scheringer, 1978; Scheringer, 1980), where the bonding density is described by a charge cloud located between bonded atoms. Negative charges are placed in the bond using a Gaussian distribution. For the valence electrons associated with the ions with partial charges (after charge transfer into the bonds), we used a new method described below to calculate scattering factors. Expansion/contraction parameters were introduced so that the radius of the outer valence electron can be expanded or contracted. This charge-cloud model provides an efficient description of the accumulation of charge in covalent bonds. The advantage of the scheme is that the numbers of parameters used to describe the charge state are small so that they can be refined directly using an optimization algorithm.

In order to accurately measure structure factors by electron diffraction, we must be able to account for the physical processes influencing the observed intensities. These include dynamical perturbations (multiple scattering), lattice vibrations, deviations from a neutral-atom model and, for organic crystals, bending of the crystals and structural modifications due to radiation damage (Dorset, 1995). The quality of the crystal also affects the observed intensities as well; in particular, the appearance of stacking faults along the short axis is likely to occur during crystallization from the gas phase. The agreement between experiment and theory will be improved significantly when all these effects are included in the theoretical model. A single diffraction pattern may not provide sufficient accuracy in the structure factors even for this known structure. We have therefore used two diffraction patterns recorded at different electron wavelengths to retrieve structure factors and our intensities were calculated using the Bloch-wave multiple-scattering method. A simulated-annealing algorithm was also used for structure refinement, using a new definition of a combined factor $R_{\rm comb}$. These will be discussed in the following sections.

The assignment of an electron scattering factor to a partially charged ion is difficult. Mitsuoka *et al.* (1999), for example, used a linear combination of scattering factors for neutral and charged atoms. However, this cannot be done unless the scattering factors for the integrally charged ion are available. Thus, in the next part of the paper, we propose a new method for calculating the scattering factors for partially charged ions. The method can be combined with an optimization algorithm for the refinement of the charge distribution.

2. Scattering factors of ions with fractional charge redistribution

Following the spherical-atom κ formalism used in X-ray crystallography (Coppens *et al.*, 1979), we have used a modified method that allows for partial charge transfer to calculate the electron scattering factors. It is possible to adjust the population and radial dependence of the valence shell by separating the scattering of the valence electrons from that of inner shells. In the κ formalism, the atomic density is written as (Coppens, 1997)

$$\rho_{\rm atom} = P_c\rho_{\rm core} + P_v\kappa^3\rho_{\rm valence}(\kappa r). \qquad (1)$$

P_c is the population of the core shell and P_v is the valence-shell population parameter, while κ is a parameter that allows expansion and contraction of the valence shell. The total number of electrons associated with the atom is equal to $P_c + P_v$. The functions $\rho_{\rm core}$ and $\rho_{\rm valence}$ are chosen as the Hartree–Fock (HF) densities of the free atoms normalized to one electron, and the valence function is allowed to expand and contract by adjustment of the parameter κ. Fourier transform of the electron density gives the X-ray scattering factor, and thus the total scattering factor for an atom, including charge transfer, can be written as

$$f^x_{\rm static}(s) = P_c f_{\rm core}(s) + P_v f_{\rm valence}(s/\kappa), \qquad (2)$$

in which $f^x_{\rm static}$ is the static X-ray scattering factor without consideration of lattice vibration. s is the scattering vector and $s = \sin\theta_B/\lambda \simeq \Theta/2\lambda$ for the reflections satisfying the Bragg condition, where θ_B is the Bragg angle and Θ is the total scattering angle.

We then use the Mott–Bethe formula to convert the resulting X-ray scattering factor into an electron scattering factor. This formula is the Fourier transform of Poisson's equation applied to an atom, and therefore relates electron and X-ray scattering factors for non-zero scattering angles. A divergence occurs for electrons scattered by ions. If the charge on the nucleus is represented as Z, then $Z_0 = \lim_{s\to 0} f^x_{\rm static}(s)$ represents the number of electrons associated with each ion or atom, for which the transferred charge is $\Delta Z = Z - Z_0$. As discussed recently by Peng (1999, and earlier workers referenced therein), the divergence of the electron scattering factor for an ion arises from the contribution of the unscreened long-range Coulomb potential, which can be represented as $\Delta Ze^2/4\pi\varepsilon_0 r$. The complete static electron scattering factor can then be calculated according to

$$f^e_{\rm static}(s) = \frac{m_0e^2}{8\pi\varepsilon_0h^2}\frac{Z_0 - f^x_{\rm static}(s)}{s^2} + \frac{m_0e^2}{8\pi\varepsilon_0h^2}\frac{\Delta Z}{s^2}. \qquad (3)$$

The term $m_0e^2/8\pi\varepsilon_0h^2 = 0.023934$ if s is given in Å^{-1} and $f^e(s)$ is in Å. At small values of s, this modified Mott–Bethe formula (Spence & Zuo, 1992) is less accurate. Then we can use a formula given by Ibers (1958):

$$f^e_{\rm static}(s) = \frac{4\pi m_0e^2}{3h^2}Z_0\overline{r^2} + \frac{m_0e^2}{8\pi\varepsilon_0h^2}\frac{\Delta Z}{s^2}, \qquad (4)$$

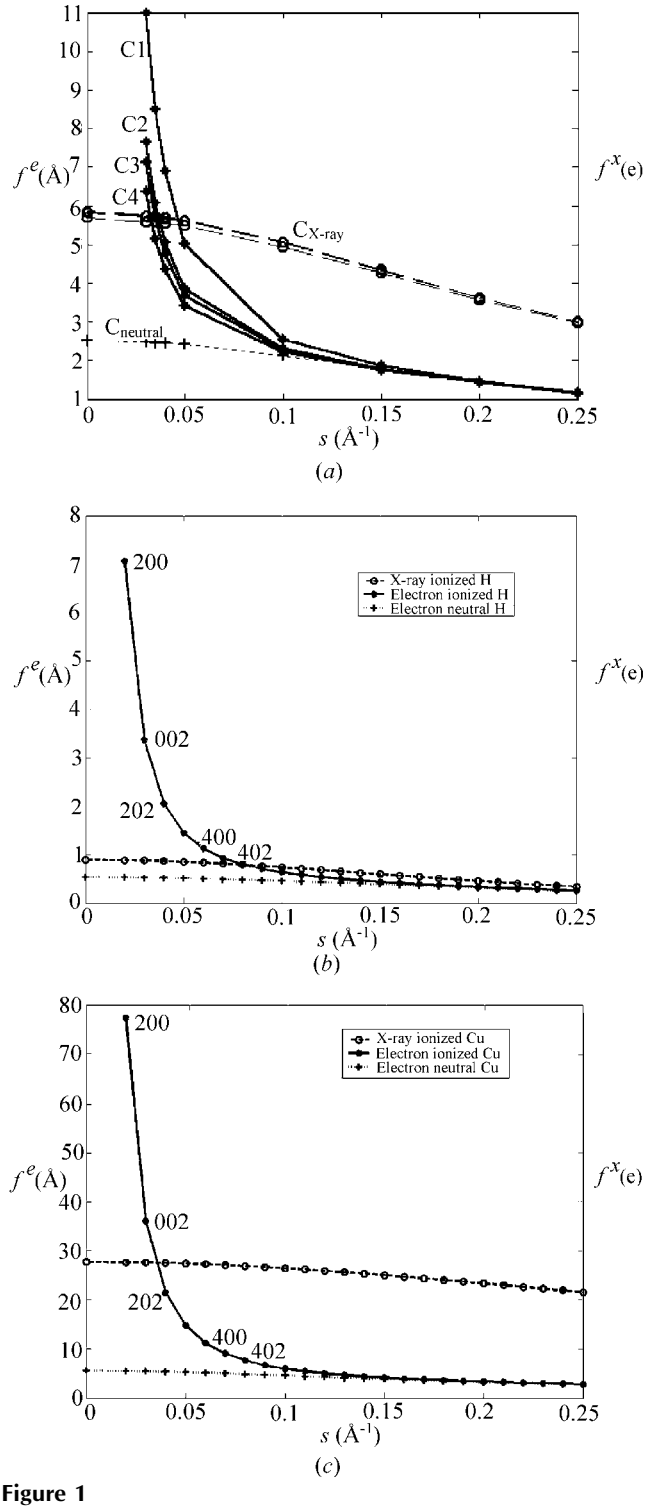

Figure 1
(*a*) Scattering factors of C: electron scattering factors of neutral C atom ($C_{neutral}$) and C ions with charges of 0.09 (C1), 0.14 (C2), 0.17 (C3) and 0.32 (C4), and X-ray scattering factors ($C_{X\text{-}ray}$) of these four C ions (the two curves are superpositions of the four curves for C1, C2, C3, C4) drawn against scattering vector *s*. (*b*) Scattering factors of H: electron scattering factors of neutral H atom, H ion with charge of 0.1053 e and its corresponding X-ray scattering factors drawn against *s*. Several low-order reflections of the α-CuPc crystal are labeled. (*c*) Scattering factor of Cu: electron scattering factors of neutral Cu atom, Cu ion with charge of 1.205 e and its corresponding X-ray scattering factors drawn against *s*. In the figure, f^e is in units of Å and *s* is in units of $Å^{-1}$, while the dimensionless f^x has the units of number of electrons.

where $\overline{r^2}$ is the mean square atomic (ionic) radius. Using these equations, the scattering factors of the separated, partially charged ions can be obtained. For example, Fig. 1 shows the electron scattering factors of the carbon ions with different fractional charges, a hydrogen ion and a copper ion. For comparison, the scattering factors of the neutral atoms and the corresponding X-ray scattering factors are also drawn in the figure.

If we consider the uncharged crystal as a whole, there is no unscreened potential. The preceeding method is equivalent to partitioning the crystal into spheres whose centers correspond to the positions of atomic nuclei. This allows us to use an isolated partially charged ion model to replace the isolated neutral atom model.

3. Fitting experimental data to dynamical calculations

For electron diffraction, dynamical scattering effects usually cannot be neglected. Given a starting structural model, we can determine how large is the dynamical effect in experimental diffraction patterns. In our simulations, we used both kinematic and dynamical methods to calculate the intensities of the reflections. Then, instead of using structure factors, we use dynamical intensities to calculate the residual for different theoretical models:

$$R = \frac{\sum_i |cI_i^{\rm cal} - I_i^{\rm exp}|}{\sum_i I_i^{\rm exp}}, \qquad (5)$$

where $I_{\rm exp}$ are the experimental intensities, $I_{\rm cal}$ are the calculated intensities and c is a normalization constant.

The simple kinematic expression implies the relationship $I_g \sim |F_g|^2$ for all observed reflections, by assuming that the scattered beams are much weaker than the incident beam and the diffracted beams scatter only once in the crystal. In this case, other parameters such as sample thickness or orientation have no influence on the calculated intensities. It is assumed here that the region illuminated in the electron microscope is smaller than one mosaic block when it is thin enough for kinematic approximation. Using the kinematic approximation, we then need only a single normalization constant: $c = \sum_i I_i^{\rm cal} / \sum_i I_i^{\rm exp}$ in order to compare experimental and calculated intensities.

An improvement in this approximation results from the introduction of excitation errors S_g since the assumption of a flat Ewald sphere introduces errors (errors introduced to high-angle reflections are larger than those of low-angle reflections). The calculated intensity is then given by

$$I_g = \frac{\lambda^2 \sin^2(\pi t S_g)}{S_g^2} |U_g|^2, \qquad (6)$$

where S_g, the distance from the Ewald sphere to the reciprocal-lattice point, can be expressed as $S_g = -(\mathbf{K}_t + \mathbf{g})^2/(2\mathbf{K})$. Here, $\mathbf{K}_t$ is the component of the incident wavevector $\mathbf{K}$ in the zero-order Laue zone, describing the tilt of the crystal. U_g is the dynamical structure factor, related to the electron structure factor F_g by $U_g = \gamma/\pi\Omega F_g$, Ω is the cell

volume, **g** is a reciprocal-lattice vector and γ is the relativistic constant. The absolute values of U_g are much smaller than those of F_g. The calculated intensity is now sensitive to the sample thickness (t) and orientation ($\mathbf{K}_t$), two parameters that do not appear in the simple kinematic approximation. If the crystal structure is known, we can use (6) to find the sample thickness and orientation by searching for the best fit between the calculated and experimental intensities. If the structure is unknown, Friedel pairs can be used to determine the kinematical thickness and orientation (Wu & Spence, 2002).

In order to account for dynamical (multiple scattering) effects, the multislice and Bloch-wave methods provide two well established methods for calculation of the intensity of reflections when an atomic structure is known. We have used the Bloch-wave theory based on matrix diagonalization of the many-beam equations (Bethe, 1928; Hirsh *et al.*, 1977; Spence & Zuo, 1992). A structure-factor matrix **A** can be written

$$\mathbf{A} = \begin{pmatrix} -K_t^2 & U_g & U_{g'} & \dots \\ U_{-g} & -(\mathbf{K}_t + \mathbf{g}')^2 & U_{h-g'} & \dots \\ U_{-g'} & U_{g-g'} & -(\mathbf{K}_t + \mathbf{g}')^2 & \dots \\ \vdots & \vdots & \vdots & \ddots \end{pmatrix},$$

in which **g**, **g**′ are reciprocal-lattice vectors for each beam. The Bloch-wave method relates the matrix **A** to a scattering matrix **S** by

$$\mathbf{S} = \exp(\pi i t \lambda \mathbf{A}). \tag{7}$$

The complex amplitudes of the spots in a diffraction pattern are given by the entries in one column of **S**. The intensities in the diffraction pattern become a complicated function of the structure factors, which describe the scattering potential.

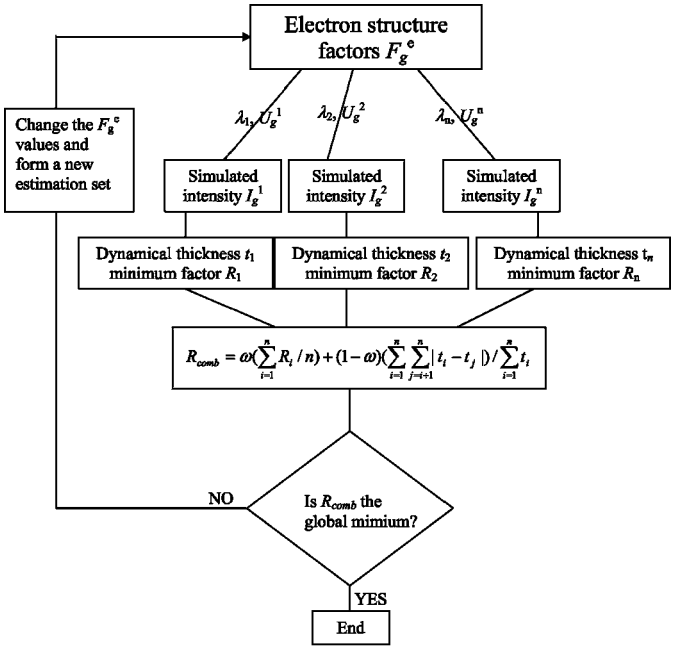

Figure 2
Flowchart of the structure-factor refinement using multiwavelength diffraction data.

4. Refinement using the charge-cloud model

In previous work (Wu & Spence, 2003), we showed how both structure factors and specimen thickness could be obtained using a multiwavelength two-beam method. Here, we use multiwavelength diffraction patterns with full dynamical calculations. The aim is to reduce the experimental errors in structure-factor refinement. The Fourier coefficients of potential V_g are properties of materials, independent of experimental parameters such as beam energy. The dynamical structure factor U_g depends on the wavelength of the incident beam, as does the scattering matrix. For a given set of experimental intensities, we can now find the specimen thickness using the Bloch-wave method if the crystal structure is known. Suppose that we have several multiwavelength patterns taken from the same crystal at the same orientation. We can then obtain a thickness for each set of observed intensities. In principle, this thickness should be the same for each pattern, and the residual calculated will decrease as the parameters approach a true description of the real crystal, for example as the effects of charge redistribution are included. Using the simulated-annealing algorithm, our algorithm searches for the best match between experimental and calculated intensities by changing the electron structure factors using the parameter-shift method. We use a combined $R_{\rm comb}$ factor and try to find the global minimum of

$$R_{\rm comb} = \omega\left(\sum_{i=1}^{n} R_i^f / n\right) + (1-\omega)\left(\sum_{i=1}^{n}\sum_{j=i+1}^{n} |t_i - t_j|\right) \Big/ \sum_{i=1}^{n} t_i, \tag{8}$$

where R_i^f is the residual for one of the i sets of experimental data as defined by Jansen *et al.* (1998). This was calculated using the observed and computed intensities:

$$R^f = \frac{\sum_i (cI_i^{\rm cal} - I_i^{\rm exp})^2}{\sum_i (I_i^{\rm exp})^2}.$$

A disadvantage of this definition of R^f is that it gives too much weight to strong reflections. This applies generally to intensities measured by electron diffraction since the errors for strong reflections are smaller than those of the weak reflections. Here t is the corresponding dynamical thickness and ω ($0 < \omega < 1$) is a weight factor. In Fig. 2, the procedure is described by a flowchart.

If the dimension of the structure-factor matrix **A** used in the Bloch-wave method is large, it becomes impossible to find the global minimum of $R_{\rm comb}$ in the high-dimensional structure-factor space using minimization algorithms. We have therefore devised a new search method. Each charge cloud between bonds has three variables: charge population, position represented by a fractional number between 0 and 1, and size (similar to isotropic temperature factor). For example, if the value of the position is 0.5, the charge cloud is situated in the middle of the bond. Instead of changing the structure-factor value of every reflection in the matrix **A** step by step, we change the charges of these charge clouds and their positions. Specimen thickness is always retained as an adjustable par-

ameter for best fit. The isotropic temperature factors were firstly refined using a neutral-atom model and their values can be refined using the charge-cloud model. Since the crystal is neutral, the total electron population must equal the sum of the nuclear charges of the constituent atoms and assumed charge clouds. During the charge refinement, the charge neutrality constraint is applied. The method we used in the refinement is to change the charges of the atoms. Then the charge populations of the 'adatoms' in the bonds can be calculated from them based on charge neutrality (see §7 for details).

Once the best model is found, its potential map can be calculated by Fourier transform of the electron structure factors F_g^e. More information can be obtained from an electron-density deformation map, which is calculated using the X-ray structure factors of the best-fit model minus those of the neutral atom aggregation model:

$$\rho_{\rm deform}(r) = \Omega^{-1} \sum_g (F^x_{\rm best\_model} - F^x_{\rm neutral\_model}) \exp(-2\pi i \mathbf{g}\cdot\mathbf{r}). \tag{9}$$

The structure factors used in (9) are X-ray structure factors converted from electron scattering factors using the Mott formula. Charge neutrality imposes the requirement that the X-ray structure factor $F(000)$ equal the number of electrons in the unit cell, independent of the charge distribution of the crystal. The Mott formula is (Spence & Zuo, 1992)

$$F_g^X = \sum_i Z_i \exp(-B_i s^2) \exp(-2\pi i \mathbf{g}\cdot\mathbf{r}_i) - (s^2/k) F_g^B, \tag{10}$$

in which F_g^X is the X-ray structure factor of reflection $\mathbf{g}$, F_g^B is the electron structure factor, r_i is the ith atomic coordinate and $k = m_0 e^2/8\pi\varepsilon_0 h^2$ a constant. In (10), we use isotropic Debye–Waller factors, for which anisotropic temperature factors may be substituted. An independent measurement of the mean inner potential by electron holography or reflection electron microscopy would provide a powerful additional constraint on the bond-charge distribution, since this quantity is extremely sensitive to bonding (Yamamoto & Spence, 1983; O'Keeffe & Spence, 1994; Kim *et al.*, 1998).

5. Error analysis

Although the introduction of a charge-cloud model in refinement may lead to a lowering of the residual $R_{\rm comb}$, the improvement is not necessarily significant because of the large number of parameters involved and results are not necessarily physically meaningful as they may be affected by parameter correlations or systematic errors in the measurement. As for the experimental intensities, we used $\sigma_i^2 = I_i^{\rm exp}$, which assumes that the statistics of the electron counting noise were Poisson. In the least-squares refinement, the standard deviation σ_{a_k} in any parameter is the root sum square of the result of the standard deviation of each data point multiplied by the effect which that data point has on the determination of the coefficient a_k (Bevington & Robinson, 1992). The condition function in the refinement we used was $F^i = I_{i\_\rm exp} - I_{i\_\rm cal}$, in which $I_{i\_\rm cal} = f(a_1, a_2, a_3, \ldots, a_p)$ represents the dynamical algorithm used to compute the simulated intensities (a_p are the p parameters varied in the refinement, such as the charge clouds and their positions). The aim is to determine the values of a_k. Our aim is to analyze the error induced in the structure factor F_g^i, which is a function of the a_k parameters: $F_g^i = g(a_1, a_2, a_3, \ldots, a_k)$. (The atomic coordinates and temperature factors are unchanged in the refinement.) The variance is (Wolberg, 1967)

$$\sigma^2_{F_g^i} = \sum_{j=1}^{p} \sum_{k=1}^{p} \left(\frac{\partial g}{\partial a_j}\right)\left(\frac{\partial g}{\partial a_k}\right) \rho_{jk} \sigma_{aj} \sigma_{ak}.$$

Since the true values of the uncertainties σ_{a_k} and the correlation coefficients ρ_{jk} are unknown, the unbiased estimates s_{a_k} and r_{jk} are used. The result will be an unbiased estimate of $\sigma^2_{F_g^i}$, and is denoted by s_f^2:

$$s_f^2 = \frac{S}{n-p} \sum_{j=1}^{p} \sum_{k=1}^{p} \left(\frac{\partial g}{\partial a_j}\right)\left(\frac{\partial g}{\partial a_k}\right) C^{-1}_{jk},$$

in which S is a weighted sum of the squares of the residuals $S = \sum_{i=1}^{n} w_{yi} R_{yi}^2$, n is the number of observed reflections and p is the number of parameters varied in the refinement. Here C^{-1}_{jk} is an element of the inverse matrix of C which is defined by

$$C_{kl} = \sum_{i=1}^{n} \frac{f_i}{\sigma_i^2} \left(\frac{\partial F}{\partial a_k}\right)\left(\frac{\partial F}{\partial a_l}\right) = C_{lk},$$

with f_i being the weight coefficient of the ith reflection. The relative stability of the refinement can also be taken as a sign of a successful refinement. As proposed by Hansen & Coppens (1978), a minimal bias of the refined parameters due to atomic asphericity is required for a reasonable refinement.

6. Experimental

The Cu-phthalocyanine films were made by sublimation in vacuum onto NaCl substrates. The substrate temperature was about 420 K. Thin films were floated onto the surface of distilled water and picked up onto copper grids. The samples were mounted in a liquid-nitrogen double-tilt goniometer TEM holder (working at 108 K) and examined using a LEO EM912 microscope with an Omega energy filter at various accelerating voltages ranging from 106 to 120 kV in steps of 2 kV. In order to reduce radiation damage, only two patterns collected at 106 and 108 kV were selected to establish a charge-cloud model for α-CuPc. We used a small illuminated area in the Koehler mode in order to minimized the dose reduce film bending. In this mode, the sample is conjugate to the illumination aperture, with a demagnification of 20. Since illumination apertures down to a few µm in diameter can be used, this mode allows selected-area patterns to be obtained from nanometre-sized areas. We moved the area of illumination away whenever we changed accelerating voltage in order to reduce irradiation damage. This was done using the microdose focusing (MDF) mode in the LEO 912 microscope, in which the illumination jumps to the area selected for

Table 1
Some of the experimental intensities read from the diffraction pattern of α-CuPc shown in Fig. 3 (taken at 120 kV), I_{exp}; calculated intensities based on a pure-kinematical approximation, I_{kine}; calculated intensities based on a kinematical approximation including excitation errors, I_{sg}; and intensities from the Bloch-wave method, I_{bloch}.

All the intensities are normalized according to $\sum_i I^i_{exp} = \sum_i I^i_{cal}$

hkl	I_{exp}	I_{kine}	I_{sg}	I_{bloch}
200	92.4434	98.1281	124.3611	83.2004
40$\bar{2}$	77.6996	65.5387	82.1459	74.5911
004	90.8414	71.5613	90.0276	82.2998
002	74.5712	79.2214	100.4076	77.4663
$\bar{2}$04	65.5717	134.0590	167.8446	67.4051
402	64.1505	110.0814	137.9756	53.7631
204	47.2141	34.2774	42.9160	51.2845
60$\bar{2}$	48.3765	7.0941	8.6170	11.2454
400	39.8112	27.5579	34.6896	39.3490
602	25.3803	12.9157	15.6884	29.3657
$\bar{2}$06	29.2260	10.7683	12.9866	27.9429
$\bar{4}$06	39.8436	3.8366	4.4827	15.4346
206	18.6246	4.0029	4.8275	8.8948
404	22.2141	8.9323	10.9871	29.2224
$\bar{2}$02	27.3382	4.1685	5.2746	20.4585
600	14.7735	4.1504	5.0856	16.8503
406	20.6823	1.5800	1.8462	6.8909
606	14.7762	31.0263	33.8733	16.4569
60$\bar{8}$	16.2271	5.6156	13.7514	12.3851
$\bar{2}$08	28.0879	20.3547	22.3210	10.9876
006	24.5577	0.9630	1.1732	9.4991

photography only for the time of the exposure. The experimental spot diffraction intensities were recorded on a cooled 14 bit 1 K × 1 K CCD camera using a YAG single-crystal scintillator as the electron detector (Spence & Zuo, 1988). The experimental intensities were retrieved with the aid of Gatan's Digital Micrograph software. The pixel intensity within a rectangle comprising the diffraction spot was firstly accumulated as the total intensity. The background quasi-elastic scattering intensity was recorded as a summation of the intensity of the pixels inside a surrounding rectangle having the same area as the former which excluded the central region of the spot. The final intensity for the spot was then obtained by subtracting the background intensity from the total intensity. The diffraction data were normalized by letting $\sum_i I^i_{exp} = \sum_i I^i_{cal}$, in which I^i_{exp} is the observed intensity and I^i_{cal} the calculated Bloch-wave intensity for the ith reflection, and the sum excludes the central beam. The Bloch-wave calculations do not include absorption. The in-column imaging energy filter in the LEO 912 is important for removing the inelastic background due to plasmon and other energy losses. A significant reduction in the background results from elastic energy filtering (Zuo *et al.*, 2000).

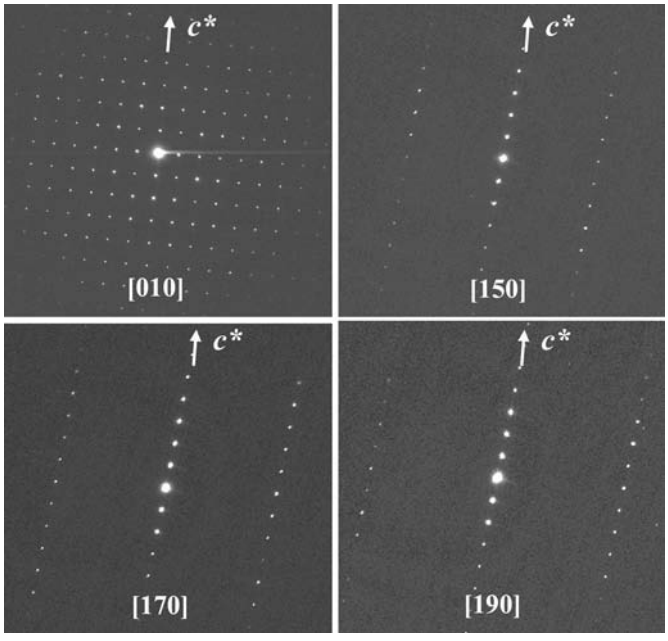

Figure 3
A series of energy-filtered electron diffraction patterns of the α-CuPc crystal tilted along the [001] direction (taken at 120 kV).

Table 2
The improvement of the fit between experimental and calculated results using different theoretical models (anisotropic Debye–Waller factors taken from β-CuPc were used).

Calculation condition	*R*	Thickness
Pure kinematic approximation	0.6568	
Kinematic approximation with S_g	0.6155	Kinematical thickness = 106 Å
Bloch-wave method and neutral-atom model	0.3128	Dynamical thickness = 218 Å

7. Results

Fig. 3 shows several diffraction patterns obtained by tilting a CuPc specimen in the microscope along the [001]* axis, from which we find that the modification of the deposited film is α-CuPc. Thus the known structure of α-CuPc (Clark *et al.*, 1979) was used as a starting model. The observed intensities were collected from the [010] spot pattern. There are altogether 78 independent *h*0*l*-type reflections, some of which are listed in the first column in Table 1. Firstly, we used a simple kinematic approximation to calculate the intensities. Then, we used a kinematic approximation that included the excitation errors, and finally a Bloch-wave method. In the three calculations, electron scattering factors for neutral atoms and anisotropic Debye–Waller factors for β-CuPc were used. The calculated intensities employing the three methods are listed in Table 1. The corresponding residual *R* factor calculated using equation (6) is also listed in Table 2 for the three methods. The simple kinematic residual *R* is 0.6568. If we include the contribution of excitation error S_g, the residual decreases to 0.6155 and the corresponding thickness at which the smallest *R* factor is produced is 106 Å. Use of the Bloch-wave multiple-scattering method brings a further large decrease in the *R* factor to 0.3128, and the corresponding thickness is 218 Å. We find that, even at these small thicknesses, multiple-scattering effects must be included for quantitative data analysis. We notice that the *R* factor is rather large. We used a large aperture in performing the tilting experiments and the crystal in the illuminated area consisted of several mosaics. Thus, the large *R* value is probably caused

by bending of the sample. Also, the orientation parameter $\mathbf{K}_t$ was not refined in these calculations. (Friedel pairs of experimental intensities were merged.) In the following, we will analyze results obtained using a much smaller aperture, collected at two beam energies, to establish the charge-cloud model.

The structure-factor matrix **A** has 58 beams in its first column and $(58 - 1) \times (58 - 1) = 3249$ beams altogether (108 are unrelated by symmetry). The dimension of the structure-factor matrix **A** depends on the size of the unit cell projected in the beam direction and on the atomic number of the atoms in the crystal. A way to test whether the number of beams is sufficient is to increase the number of beams and ensure that this increase makes no appreciable difference to the intensities of the beams of interest (Cowley, 1992). Meanwhile, weak beams can be included using the 'Bethe perturbation' method (Zuo & Weickenmeier, 1995). For example, Fig. 4 plots two sets of $I \sim t$ *Pendellösung* curves for the $(\bar{2}04)$ and (200) beams, for two structure-factor matrices **A**. The first has dimension 58 and 222 additional beams incorporated by Bethe perturbation, while the other has 72 beams treated exactly and an additional 204 beams by Bethe perturbation. Their difference may be evaluated using chi-square $\chi^2 = \sum_i (1/I_i^2)(I_i^2 - I_i^1)^2$, giving $\chi^2_{(\bar{2}04)} = 0.56$ and $\chi^2_{(200)} = 0.05$. We have therefore used a matrix **A** containing 58 beams in its first column and 222 beams treated by Bethe perturbation. The orientation parameter $\mathbf{K}_t$ is not included since the diffraction intensities were read from a zone-axis pattern.

We now consider incorporating the charge-cloud model refinement with the Bloch-wave scheme. To do this, we used two electron diffraction patterns along the [010] direction taken at 106 and 108 kV from the same crystal as shown in Fig. 5. In the calculations, we included only 36 low-angle reflections with $s < 0.12$ because the electron diffraction method is not very accurate for the determination of high-angle reflections. Friedel pairs in the raw data were not merged. Accordingly, we introduced orientation parameters $\mathbf{K}_t$ in the Bloch-wave method. We used the neutral-atom model to get the best-fit values of $\mathbf{K}_t$ from high-order reflections. (The $\mathbf{K}_t$ values remain unchanged in the charge-cloud model refinement.) Fig. 6(*a*) shows the residual *R* factor varying with specimen thickness by using the neutral-atom aggregation model. For the two sets of data, the smallest R^f are 0.0749 and 0.0718 with the corresponding thicknesses being 389 and 389 Å, respectively. We then employed the charge-cloud model to do the refinement by searching for a smaller $R_{\rm comb}$ for the two sets of observed

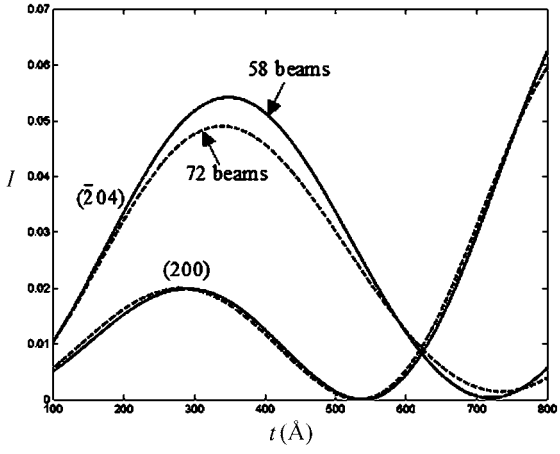

Figure 4
Pendellösung curves ($I_g \sim t$) of **g** = $(\bar{2}04)$ and **g** = (200) calculated using 58 beams (solid line) and 72 beams (dashed line) in the first column of the structure-factor matrix **A**.

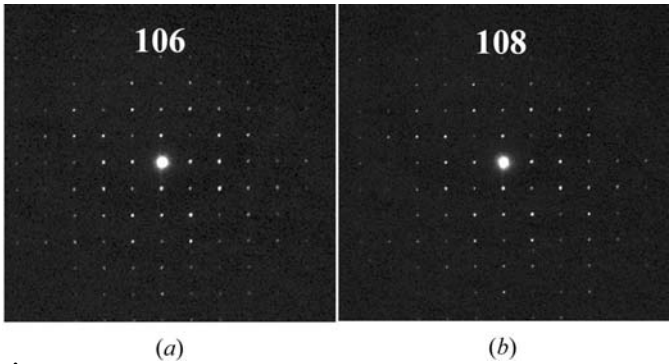

Figure 5
Two diffraction patterns used for refinement of the charge-cloud model with the experimental voltages labeled: (*a*) 106 kV, (*b*) 108 kV.

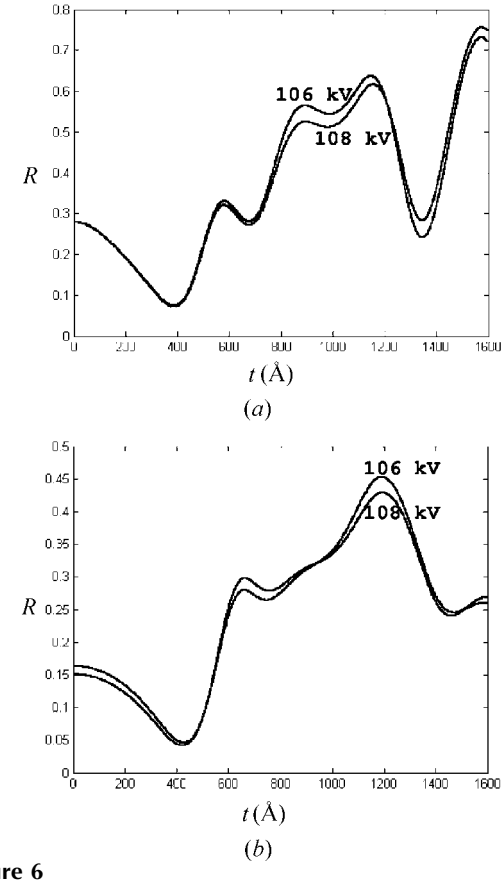

Figure 6
The calculated residual R^f for two sets of intensities collected at accelerating voltages of 106 and 108 kV (indicated in the figure) using the Bloch-wave method against theoretical specimen thickness *t* of (*a*) the neutral-atom model of the α-CuPc structure and (*b*) the charge-cloud model. Using this optimization, the sample thickness can be determined.

Table 3
Experimental intensities (at 108 kV) read from the diffraction pattern of α-CuPc shown in Fig. 5(*a*), I_{exp}; calculated intensities based on the neutral atomic model, I_{neu}; calculated intensities based on the charge-cloud model, I_{charge}.

All the intensities are normalized according to $\sum_i I^i_{exp} = \sum_i I^i_{cal}$.

hkl	I_{exp}	I_{neu}	I_{charge}
200	2.763	2.606	2.794
002	2.483	2.491	2.514
$\bar{2}02$	0.473	0.614	0.462
202	0.355	0.458	0.349
400	1.115	1.012	1.173
004	2.463	2.358	2.389
$40\bar{2}$	2.638	2.136	2.487
402	2.014	2.038	1.905
$\bar{2}04$	2.244	2.334	2.335
204	1.354	1.277	1.368
$\bar{4}04$	0.289	0.382	0.302
404	0.624	0.768	0.616

Table 4
Atomic charges, and charges and positions for adatoms obtained from the best charge-cloud model of the α-CuPc structure.

The position parameters measure the distance from the first atom to the second atom, *i.e.* the adatom is near the first atom if the value is smaller than 0.5.

Atoms	Electrons	Adatoms	Electrons	Position	Isotropic U (Å^2)
Cu	27.79 (5)	Cu-N1	0.30 (55)	0.54 (5)	0.99 (1)
N1	6.98 (73)	N1—C1	0.14 (83)	0.49 (9)	0.95 (7)
N2	6.86 (32)	N2—C1	0.21 (25)	0.47 (8)	0.95 (7)
C1	5.56 (77)	C1—C2	0.24 (41)	0.46 (9)	0.95 (4)
C2	5.70 (1)	C2—C3	0.25 (67)	0.49 (2)	0.98 (2)
C3	5.53 (1)	C3—C4	0.27 (50)	0.50 (6)	0.97 (6)
C4	5.64 (5)	C4—C4	0.23 (67)	0.44 (3)	0.97 (6)
H1	0.88 (72)	C2—C2	0.20 (1)	0.44 (1)	0.98 (8)
H2	0.89 (1)	C4—H1	0.23 (11)	0.56 (1)	0.95 (6)
		C3—H2	0.26 (67)	0.55 (7)	0.98 (1)

intensities. The projection of the structure of α-CuPc along the [010] direction is shown in Fig. 7. One CuPc molecule has a pseudofourfold axis (chemical symmetry). Thus we used only nine independent atoms, labeled in Fig. 7 as Cu, C1, C2, C3, C4, N1, N2, H1 and H2, to do the charge refinement. The Gaussian charges placed along the bond were then calculated from the charges of the associated atoms contributing to the bond according to the rule of charge neutrality. For example, there are four Cu—N1 bonds, one Cu atom and four N1 atoms in a CuPc molecule. The charge transfer from Cu contributes completely to the Cu—N1 bond but only 1/3 of the total charge transfer of N1 contributes to the Cu—N1 bond. Thus the charge population for the Cu—N1 bond can be calculated using the sum of the charge transfers of one Cu and four N1 divided by 4. For each charge cloud situated at the bonds, a size parameter (like the isotropic temperature factor) was used to describe the expansion or contraction of the charge cloud. At the same time, the position parameters of each bond charge and sample thickness t were also treated as refinement parameters. The refinement results are shown in Fig. 6(*b*).

Table 5
List of the electron structure factors (F_g^e) and X-ray structure factors (F_g^X) derived from the best matched charge-cloud model and neutral-atom model.

F_g^X values were calculated using the Mott formula.

		Electron structure factors F_g^e		X-ray structure factors F_g^X	
hkl	*s*	Best ion model (Å)	Neutral model (Å)	Best ion model (e Å^{-3})	Neutral model (e Å^{-3})
200	0.0386	66.74	70.67	266.43	269.77
002	0.0418	59.93	63.67	249.35	253.28
$\bar{2}02$	0.0567	6.88	15.12	116.29	118.97
202	0.0571	2.40	10.52	102.74	104.32
400	0.0772	−25.12	−37.54	−24.82	−29.19
004	0.0836	−42.45	−58.95	−75.69	−78.47

Using the charge-cloud model of CuPc, for the two sets of data with accelerating voltages of 106 and 108 kV (indicated in Fig. 6), the smallest R^f are 0.0426 and 0.0432, both with a corresponding thickness of 418 Å. The observed and calculated intensities with the neutral and charge-cloud models are listed in Table 3. The corresponding atomic charges and the positions of atoms and bond charges are listed in Table 4. It was reasonable that they should have the same dynamical thickness since the diffraction came from the same crystal and the same area. Furthermore, the decrease of the R^f factors for the two patterns means that the charge-cloud model is better than the neutral-atom model for calculating the structure factors.

The electron structure factors calculated by the neutral-atom model and the ionic model are shown in columns 1 and 2

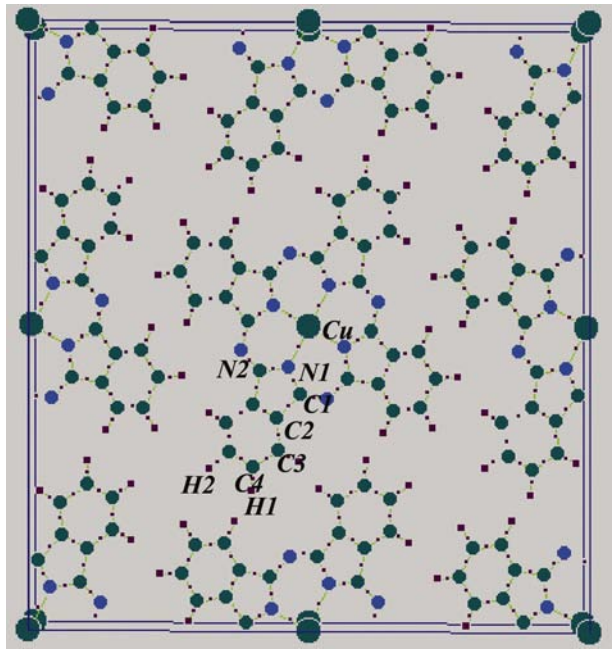

Figure 7
Projection of the α-CuPc structure along the [010] direction. The independent atoms used for charge refinement are labeled. The 'adatoms' situated at the middle of the bonds (position parameter 0.5) are also drawn. (Powder cell; Nolze & Kraus, 1998).

in Table 5. For the low-angle reflections (*i.e.* $s < 0.1$ Å^{-1}), the deviations of the structure factors between the two models are large. In order to show a deformation-density map using the ionic model, we used the Mott formula to transform the electron structure factors to X-ray structure factors. The calculated X-ray structure factors are also listed in Table 5 (columns 3 and 4). For the same low-angle reflections, the differences between the X-ray structure factors calculated using the charge-cloud model and those calculated using the neutral model are smaller. This shows that electron diffraction is more sensitive to charge redistribution in the low-angle region. Meanwhile, it should be noted that there is ample evidence that bonding effects are important to at least s = 0.8–0.9 Å^{-1} (Coppens, 1997), which influences the structure factors of many reflections. Fig. 8 shows the best-fit structure factors with error bars compared to the structure factors calculated using the neutral-atom model. The error was calculated using the method introduced above in §5.

The deformation charge-density map calculated by Fourier transform of the difference between the best ionic model and the neutral-atom model is shown in Fig. 9(*a*). It was obtained by subtraction of the charge density for neutral atoms from the total charge density based on refined structure factors. Each contour line represents an increment of 0.12 e Å^{-3}. The deformation map is compared to the *ab initio* calculated deformation map shown in Fig. 9(*b*). A theoretical calculation was performed using a full-potential (linearized) augmented plane wave (LAPW) (plus local orbitals) algorithm, as embodied in the *WIEN2K* algorithm (Schwarz *et al.*, 2002). Muffin tin radii used were 1.8 a.u. for the Cu atom, 1.2 a.u. for the C atom and 0.6 a.u. for the H atom. There is a difference in these two maps around the Cu atom, and the deformation density of an N lone pair shown in the theoretical map does not appear in the map of Fig. 9(*a*). Noise in the experimental data may account for this. Also, the relatively small values of the parameters refined in our algorithm reduces the accuracy of the method, although the main features of charge transfer in the CuPc molecule can be seen.

8. Discussion

This procedure for finding accurate structure factors from a dynamical electron diffraction pattern is similar to the refinement of a structural model. Both are dependent on the gradual reduction of the difference between the calculated and experimental intensities, using an optimization method. However, for the usual case of multiple scattering, the intensity of a particular Bragg beam depends on many factors such as sample thickness, absorption coefficients, orientation, accelerating voltage, degree of beam damage, structure factors. The vast parameter space makes the optimization process impossible, especially when the number of observed diffraction intensities is small. For example, in the case of the α-CuPc crystal, a 58-beam structure-factor matrix has 108 independent beams, whose structure factors are all influenced by bond formation since their scattering vectors s are less than 0.8. Even a crude search of the whole parameter space by a meshed grid and step-by-step adjustment of the 108 structure factors is impossible using currently available optimization programs. In order to reduce the number of parameters to be refined, we have used an isolated partially charged ionized atom model. The deformation-density map is calculated by comparing the charge-cloud model with the neutral-atom model. In addition, our use of multiple

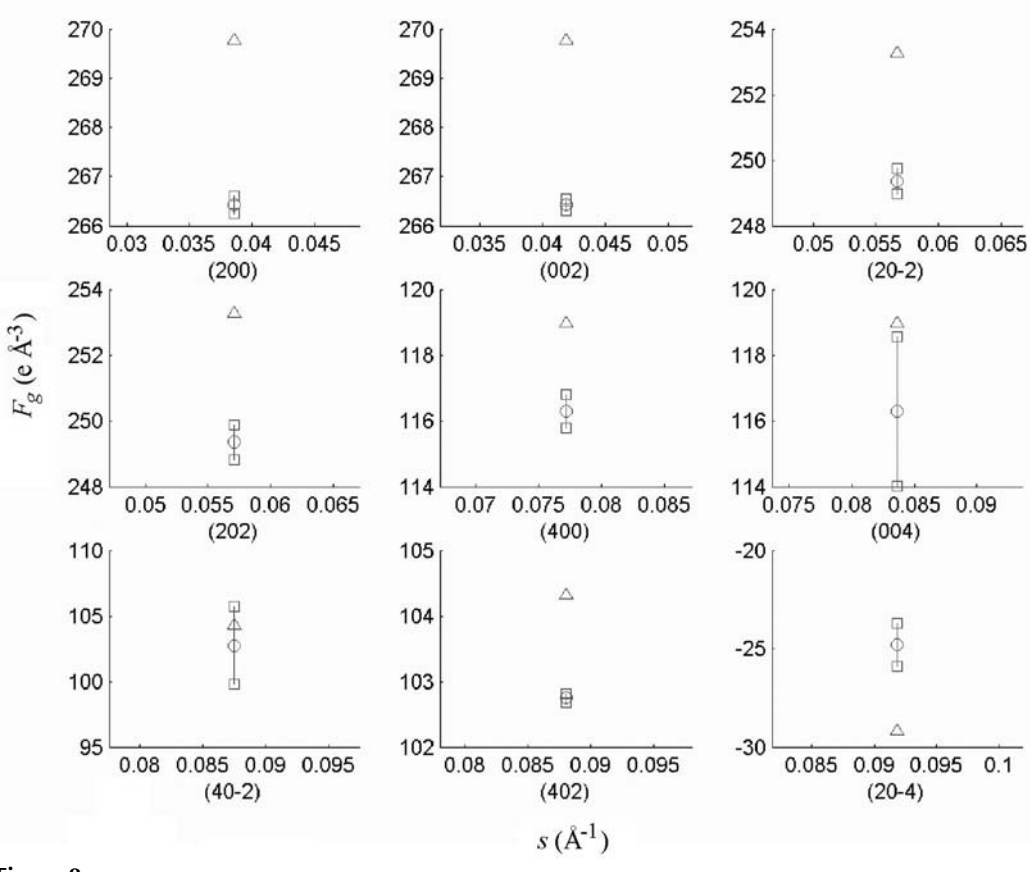

Figure 8
The best-fit X-ray structure factors (circles) with their errors, compared to those for a neutral-atom model (triangles) for nine low-order reflections.

electron wavelengths and a molecule of known structure greatly reduce the severity of the global optimization problem.

For organic molecular crystals with large unit cells, quantitative electron diffraction combined with full dynamical calculation therefore has the ability to study bonding effects. This is mainly because the electron scattering factors (and thus structure factors) of the low-order reflections ($s < 0.15$) deviate greatly from the values of neutral atoms – much more so than for X-ray diffraction (Spence & Zuo (1992). Since the number of parameters included in a least-squares refinement must be limited, the shape of each mid-bond charge was not refined. Thus, the method is semiquantitative and not as accurate as, for example, quantitative convergent-beam analysis from inorganic crystals, where the many turning points of the rocking curve within each Bragg order can be used for refinement (Spence & Zuo, 1992). A more precise procedure would be the introduction of multipole functions to describe the valence-electron distribution (Coppens *et al.*, 1979). However, the number of parameters to be refined using multipole functions is also too large for a complex structure with 29 independent atoms in its asymmetric unit cell. A better approach for representing the charge distribution with high accuracy and few refinable parameters is crucial for the study of bonding in structures with large unit cells.

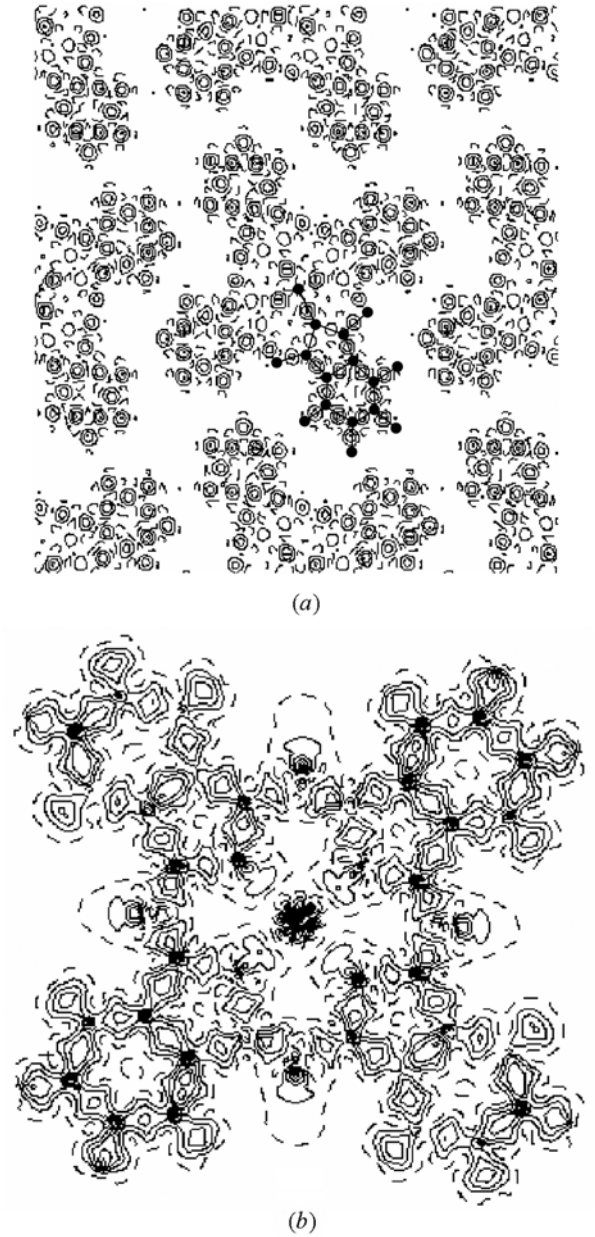

Figure 9
Deformation charge-density maps of α-CuPc in the (010) plane (*a*) Total charge density from the refined structure factors of the charge-cloud model minus the charge density for neutral atoms. Contours are at 0.12 e Å^{-3}. Negative contours are broken lines. (*b*). *Ab initio* calculated map, performed using the *WIEN2K* program (Schwarz *et al.*, 2002). Contours are at 0.1 e Å^{-3}. Negative contours are broken lines.

9. Conclusions

Several important factors that influence experimental electron diffraction intensities from thin organic crystals, such as multiple scattering and charge redistribution, have been considered in relation to α-CuPc. A flexible method for calculation of scattering factors of partially charged ions has been proposed. A mid-bond charge-cloud ionic model which describes both ionicity and covalency was used, and shown to greatly improve the fit between experimental and observed intensities in spot diffraction patterns. The best ionic model was found using an optimization algorithm to refine multi-wavelength electron diffraction patterns. A charge distribution for the α-CuPc crystal has been obtained. This suggests that convergent-beam data may not be needed for a simplified analysis of bonding in radiation-resistant organic crystals of partially known structures.

This work is supported by ARO award DAAD190010500.

References

Ashida, M., Uyeda, N. & Suito, E. (1966). *Bull. Chem. Soc. Jpn*, **39**, 2616–2624.
Bethe, H. A. (1928). *Ann. Phys. (Leipzig)*, **87**, 55–129.
Bevington, P. R. & Robinson, D. K. (1992). *Data Reduction and Error Analysis for the Physical Sciences*, 2nd ed. New York: McGraw-Hill.
Brill, R. (1960). *Acta Cryst.* **13**, 275–276.
Brown, C. J. (1968*a*) *J. Chem. Soc. A*, pp. 2488–2493.
Brown, C. J. (1968*b*). *J. Chem. Soc. A*, pp. 2494–2498.
Clark, W. R. K., Chapman, J. N. & Ferrier, R. P. (1979). *Nature (London)*, **277**, 368–370.
Coppens, P. (1997). *X-ray Charge Density and Chemical Bonding.* IUCr/Oxford University Press.
Coppens, P., Guru Row, T. N., Leung, P., Stevens, E. D., Becker, P. J. & Yang, Y. W. (1979). *Acta Cryst.* A**35**, 63–72.
Cowley, J. M. (1992). *Techniques of Transmission Electron Diffraction.* New York: Oxford University Press.
Cowley, J. M. & Rees, A. L. G. (1947). *Proc. Phys. Soc. London*, **59**, 283.
Dietrich, H. & Scheringer, C. (1978). *Acta Cryst.* B**34**, 54–63.
Dorset, D. L. (1995). *Structural Electron Crystallography*. New York: Plenum Press.
Dorset D. L. & Hauptman H. A. (1976). *Ultramicroscopy*, **1**, 195–201.
Dorset, D. L., Jap, B. K., Ho, M. H. & Glaeser, R. M. (1979). *Acta Cryst.* A**35**, 1001–1009.

Hansen, N. K. & Coppens, P. (1978). *Acta Cryst.* A**34**, 909–921.
Hellner, E. (1977). *Acta Cryst.* B**33**, 3813–3816.
Hirsh, P. B., Howie, A., Nicholson, R. B., Pashley, D. W. & Whelan, M. J. (1977). *Electron Microscopy of Thin Crystals*, 2nd ed., pp. 208–210. Florida: Krieger; London: Butterworth.
Ibers, J. A. (1958). *Acta Cryst.* **11**, 178–183.
Jansen, J., Tang, D., Zandbergen, H. W. & Schenk, H. (1998). *Acta Cryst.* A**54**, 91–101.
Kim, M. Y., Zuo, J. M. & Spence, J. C. H. (1998). *Phys. Status Solidi A*, **166**, 445–451.
Mitsuoka, K., Hirai, T., Murata, K., Miyazawa, A., Kidera, A., Kimura, Y. & Fujiyoshi, Y. (1999). *J. Mol. Biol.* **286**, 861–882.
Murata, Y., Fryer, J. R. & Baird, T. (1976). *J. Microsc.* **108**, 261–275.
Nolze, G. & Kraus, W. (1998). *Powder Diffr.* **13**, 256–256.
O'Keeffe, M. & Spence, J. C. H. (1994). *Acta Cryst.* A**50**, 33–45.
Peng, L. M. (1999). *Micron*, **30**, 625–648.
Robinson, M. T. & Klein, G. E. (1952). *J. Am. Chem. Soc.* **74**, 6294.
Scheringer, C. (1980). *Acta Cryst.* A**36**, 205–210.
Schwarz, K., Blaha, P. & Madsen, G. K. H. (2002). *Comput. Phys. Commun.* **147**, 71–76.
Spence, J. C. H. & Zuo, J. M. (1988). *Rev. Sci. Instrum.* **59**, 2102–2105.
Spence, J. C. H. & Zuo, J. M. (1992). *Electron Microdiffraction.* New York and London: Plenum Press.
Uyeda, N., Ashida, M. & Suito, E. (1965). *J. Appl. Phys.* **36**, 1453–1460.
Vainshtein, B. K. (1964). *Structure Analysis by Electron Diffraction.* Oxford: Pergamon Press.
Wolberg, J. R. (1967). *Prediction Analysis.* Princeton: Van Nostrand; New York: Plenum Press.
Wu, J. S. & Spence, J. C. H. (2002). *Acta Cryst.* A**58**, 580–589.
Wu, J. S. & Spence, J. C. H. (2003). *Microsc. Microanal.* In the press.
Yamamoto, N. & Spence, J. C. H. (1983). *Thin Solid Films*, **104**, 43–55.
Zhong, S. J., Dadarlat, V. M., Glaeser, R. M., Head-Gordon, T. & Downing, K. H. (2002). *Acta Cryst.* A**58**, 162–170.
Zuo, J. M. (2000). *Microsc. Res. Tech.* **49**, 245–268.
Zuo, J. M., Kim, M., O'Keeffe, M. & Spence, J. C. H. (1999). *Nature (London)*, **401**, 49–52.
Zuo, J. M., Pacaud, J., Hoier, R. & Spence J. C. H. (2000). *Micron*, **31**, 527–532.
Zuo, J. M., Spence, J. C. H. & O'Keeffe, M. (1988). *Phys. Rev. Lett.* **61**, 353–356.
Zuo, J. M. & Weickenmeier, A. L. (1995). *Ultramicroscopy*, **57**, 375–383.